VHF/UHF Open-sleeve Dipole Antenna Array for Airborne Ice Sounding and Imaging Radar

Hoyun Won, Yang-Ki Hong, Linfeng Li, Abhishek Awasthi, Natalie Nickerson, Briana Bryant, Minyeong Choi, Jie-Bang Yan, *Senior Member*, *IEEE*, Drew Taylor, Charles O'Neill, and Joohan Lee

Abstract—This paper presents a simple, lightweight, and ultrawideband, VHF/UHF open-sleeve dipole antenna array for airborne ice measuring radar. The proposed antenna array achieves a wide bandwidth of 300 MHz via mutual coupling from neighboring excited elements. A hollow aluminum tube is used for both dipole and parasitic elements to minimize the antenna's weight. The simulation results show that to achieve a bandwidth of 300 MHz with a peak realized gain up to 12 dBi in the frequency range from 170 to 470 MHz, the length of the dipole (L_{dip}) and parasitic elements (L_{para}) of elements 1 and 4 of the 4-element antenna array need to be 670 mm and 200 mm, respectively. At the same time, elements 2 and 3 require a L_{dip} of 640 mm and L_{para} of 180 mm. Based on these dimensions, a 4-element antenna array is fabricated and tested. The measured antenna performance results show a good agreement with the simulated results.

Index Terms—Ice sounding radar, VHF/UHF antenna, Open-sleeve dipole antenna, Antenna arrays

I. INTRODUCTION

Observations of polar ice sheets are crucial for estimating ice sheets' contribution to sea-level rise, which causes coastal flooding, salinity changes, and changes in marine habitat [1]. Lidar, gravimetry, seismic experiments, and airborne radar have been employed to study ice dynamics in the polar region [2]. Among these established methods, airborne radar with ultra-wideband (UWB) VHF/UHF RF system is the most promising solution for imaging the ice stratigraphy due to its fine-resolution mapping and high measurement accuracy [2].

To transmit and receive such UWB signals, many UWB VHF/UHF antennas were developed [2-5]. Rodriguez-Morales *et al.* [2] and A. Fenn *et al.* [3] presented a 12-element folded dipole and 24-element dipole antenna array, respectively.

Hoyun Won, Yang-Ki Hong, Linfeng Li, Abhishek Awasthi, Briana Bryant, Minyeong Choi, Jie-Bang Yan., and Drew Taylor are with Department of Electrical and Computer Engineering and Remote Sensing Center, The University of Alabama, Tuscaloosa, AL 35487 USA. (e-mail: hwon@crimson.ua.edu, ykhong@eng.ua.edu, lli74@crimson.ua.edu, aawasthi1@eng.ua.edu, bmbryant1@crimson.ua.edu, mchoi11@crimson.ua.edu, jbyan@ua.edu, rtaylor@eng.ua.edu).

Natalie Nickerson is with Department of Aerospace Engineering and Mechanics and Remote Sensing Center, The University of Alabama, Tuscaloosa. AL 35487 USA. (email: njnickerson@crimson.ua.edu).

Charles O'Neill is with Aerofluids, College Station, TX 77842 USA. (email: oneill@aerofluids.com).

Joohan Lee is with Department of Future Technology Convergence, Korea Polar Research Institute, Incheon, South Korea (e-mail: joohan@kopri.re.kr)
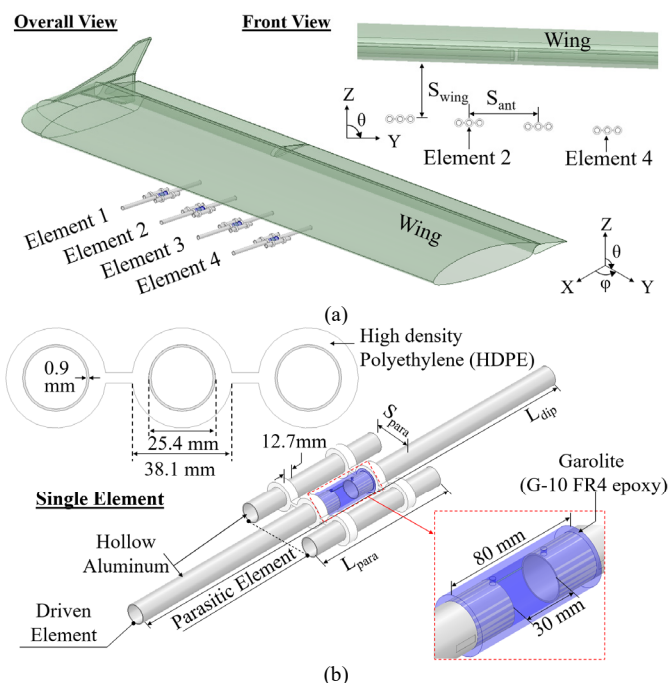
Fig. 1. (a) Overall view of the 4-element open-sleeve dipole antenna array under wing and (b) open-sleeve dipole antenna geometry and specification.

Although the arrays' structures are simple, the arrays suffer from narrow bandwidths of 60 MHz and 40 MHz, respectively. Yan *et al.* [4] reported a 16-element low-profile planar dipole antenna array that operates between 150 and 500 MHz, while I. Tzanidis et al. [5] designed a 7×7 tightly coupled dipole array that operates between 200 and 600 MHz. Despite their wide bandwidths, the reported arrays require an intricate and heavy antenna enclosures for airborne operation.

This letter reports a simple, lightweight, UWB, and high gain open-sleeve dipole antenna (ODA) array for an airborne VHF/UHF radar. The proposed antenna array realizes a required bandwidth of 300 MHz and peak realized gain (RG_{peak}) of 10 dBi or higher across the range of 170 to 470 MHz to achieve a radar resolution of 0.5 m and signal-to-noise ratio of 10 dB, respectively. We describe the proposed ODA array configuration first and then its simulated and measured antenna performances in the following sections. A three-dimensional (3-D) finite element simulator (ANSYS HFSS ver. 2019 R2) was used to evaluate antenna performance.

II. ANTENNA DESIGN AND SIMULATION RESULTS

Fig. 1 shows the geometry and dimensions of the optimized

TABLE I. DIMENSIONS OF OPTIMIZED 4-ELEMENT OPEN-SLEEVE DIPOLE ANTENNA ARRAY

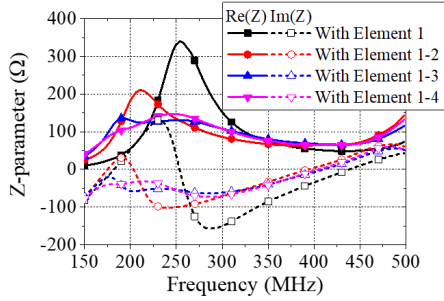| Parameter	Value	
	Element 1 and 4	Element 2 and 3
Length of dipole element (L_{dip})	670 mm	640 mm
Length of parasitic element (L_{para})	200 mm	180 mm
Separation between dipole and parasitic element (S_{para})	48 mm	
Separation between wing and antenna (S_{wing})	270 mm	
Separation between antennas (S_{ant})	317.5 mm	

TABLE II. REAL AND IMAGINARY PART OF SELF, MUTUAL, AND ACTIVE IMPEDANCE AT 230 MHZ

Impedance	Z_{11}	Z_{12}	Z_{13}	Z_{14}	Z_{1d}
Real part	148.3	70.0	-51.8	-60.7	105.7
Imaginary part	70.0	-98.9	-50.4	65.5	2.7

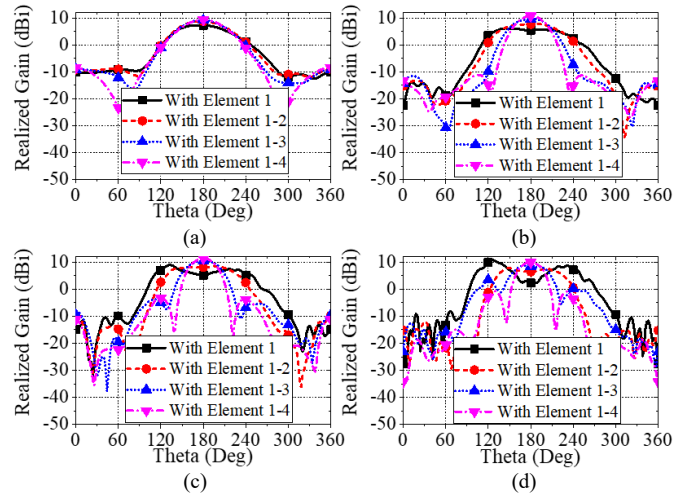Fig. 2. Real and imaginary part of the impedance of the element 1 with increasing number of elements.

Fig. 3. Simulated radiation pattern of the 4-element open-sleeve antenna array at (a) 170 MHz, (b) 320 MHz, (c) 400 MHz, and (d) 470 MHz in yz-plane.
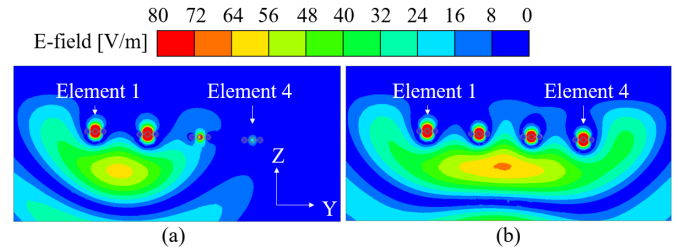

Fig. 4. E-field distribution at 400 MHz for N_{ant} of (a) 2 and (b) 4 in yz-plane.

4-element ODA array mounted under the aircraft left wing. The antenna consists of a dipole antenna with a center feed and parasitic elements on each dipole side. We selected a commercial 1" diameter and 0.035" thick hollow aluminum tube for dipole and parasitic elements to minimize the mechanical stress on the wing and maximize the airborne survey range. Further, to observe the antenna performance more realistically, a realistic metal wing model (1300 mm wide, 3700 mm long, and 150 mm thick) was adopted as shown in Fig. 1. The detailed dimensions of the ODA array are given in Table I.

A. Antenna Element and Balun Design

First, we investigated the input feed impedance of the 4-element ODA array. Fig. 2 shows the active real and imaginary parts of the impedance of element 1 with respect to the increase in the number of excited elements (N_{ant}). For a single excited element, the real part of the input impedance exponentially increases from 0 to 340 Ω between 150 and 250 MHz and decreases from 340 to 50 Ω afterward, while the imaginary part fluctuates between 120 and -150 Ω across the operating frequencies. As the N_{ant} increases from 2 to 4, less fluctuation in the real and imaginary parts of the impedance is observed. This is mainly attributed to mutual coupling between neighboring antennas, which changes the active impedance of the antenna (Z_{ad}) [6,7]. The Z_{ad} is calculated as follows

$$Z_{ad} = Z_{a1} + Z_{a2} + \cdots + Z_{an} \qquad (1)$$

where $a=1,2,\cdots, n$ and n is the total N_{ant}. Table II shows the real and imaginary part of the self, mutual, and resultant active impedances at 230 MHz. It shows that the mutual impedances affect the resultant Z_{ad} significantly by changing the real and imaginary parts of the Z_{ad} close to 100 and 0 Ω, respectively. Based on these simulation results, a feed impedance of 100 Ω is chosen in order to achieve a bandwidth of 300 MHz.

In addition, the mutual coupling also affects the realized gain radiation pattern significantly. Fig. 3 shows the simulated radiation pattern at various frequencies with respect to increase in the N_{ant} in the yz-plane. With the single element excited, the radiation pattern shows a beam split that diverges as the frequency increases. This is because the ratio of the S_{wing} to wavelength (λ) exceeds $\lambda/4$ as reported in [7]. However, as the N_{ant} increases, this split radiation pattern changes to a broadside radiation pattern. This is mainly attributed to the change in total radiated field from excited elements as follows [8]

$$E(r,\theta,\phi) = \frac{e^{-jkr}}{r}\left[b_1 f_1(\theta,\phi) + b_2 f_2(\theta,\phi) + \cdots + b_n f_n(\theta,\phi)\right] \quad (2)$$

where $k = 2\pi/\lambda$, r is the distance between antenna and observer, and b_n and f_n are the amplitude and field components of the outgoing wave when antenna n is excited, respectively. Accordingly, each antennas' radiation fields add up and change the total radiated field, as shown in Fig. 4 in the yz-plane. Similar electric field (E-field) distribution was observed in the xz-plane and for H-field in both planes (not shown).

To feed the dipole with a 100 Ω impedance, a 100 W 1:2 balun was designed and fabricated. Fig. 5 shows the designed balun and its measured performance. A standard 50 Ω SMA connector is first split into two 25 Ω lines via a 1:1 balun. Then,
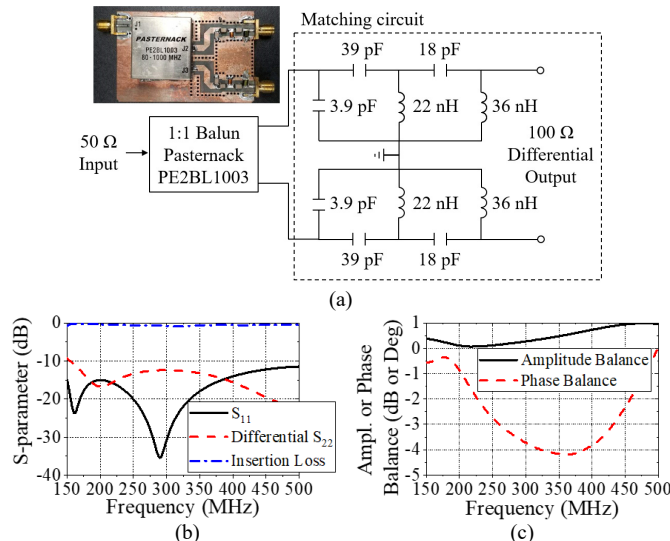
Fig. 5. (a) Circuit schematic of the 1:2 balun and measured (b) input and output S-parameter and insertion loss and (c) amplitude and phase balance.
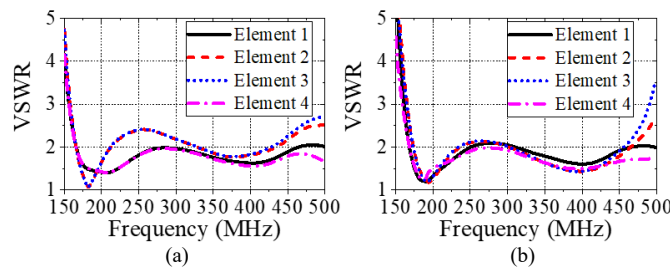

Fig. 6. Simulated active VSWR of the 4-element open-sleeve antenna array with (a) L_{dip} of 670 mm and L_{para} of 200 mm for all element and (b) L_{dip} of 670 mm and L_{para} of 200 mm for element 1 and 4 and L_{dip} of 640 mm and L_{para} of 180 mm for element 2 and 3.
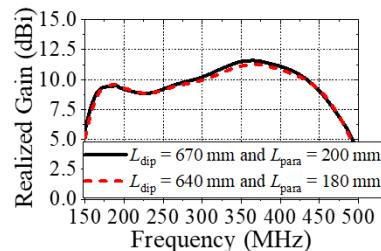

Fig. 7. Simulated realized gain at boresight of the 4-element open-sleeve antenna array with initial and optimized dimensions.

these two 25 Ω are connected to a matching circuit that consists of an inductor and capacitor to convert to a 100 Ω differential output. The balun's measured results show a good return loss of more than 12 dB for both input and output, a low insertion loss of less than 0.5 dB, and an acceptable amplitude and phase balance of less than 1 dB and 4.1 degrees, respectively.

B. Antenna Design Parametric Study

Initially, we simulated the array with identical antenna elements of the following dimensions: L_{dip} of 670 mm, L_{para} of 200 mm, S_{para} of 48 mm, S_{wing} of 270 mm, and S_{ant} of 317.5 mm for antenna performances. Fig. 6 (a) shows the corresponding simulated active voltage standing wave ratio (VSWR) of the 4-element ODA array. As shown, the VSWRs of elements 1 and 4 are below 2 from 170 to 470 MHz. Although the first crossing frequency of the active VSWR below 2 (f_{first}) occurs at 170
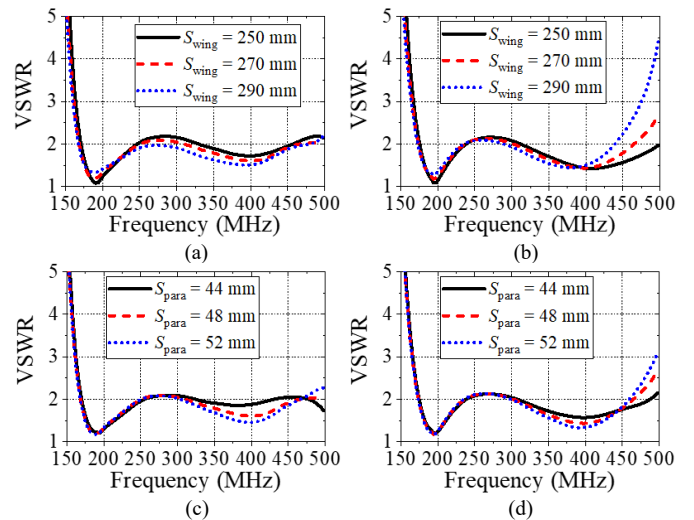

Fig. 8. Simulated active VSWR of the 4-element open-sleeve dipole antenna array with various S_{wing} for element (a) 1 and (b) 2 and various S_{para} for element (c) 1 and (d) 2.
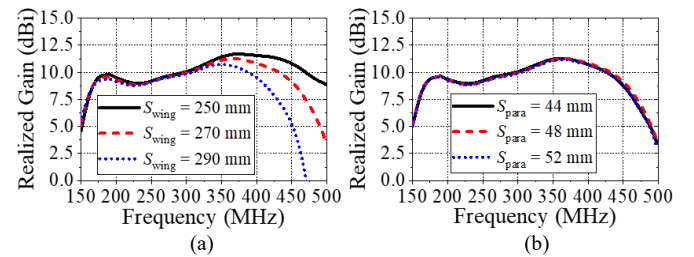

Fig. 9. Simulated realized gain at boresight of the 4-element open-sleeve antenna array with various (a) S_{wing} and (b) S_{para}.

MHz for elements 2 and 3, the VSWR of elements 2 and 3 exceeds 2 when the operating frequency is between 214 and 326 MHz and above 430 MHz.

To reduce the VSWR of element 2 and 3 below 2, the L_{dip} and L_{para} of elements 2 and 3 are reduced from 670 to 640 mm and 200 to 180 mm, respectively, without altering the other dimensions. These changes reduce the VSWR of elements 2 and 3 from 2.4 to 2.1 in the band of interest as illustrated in Fig. 6 (b). The main reason for this reduction is that the shorten L_{dip} and L_{para} increase the first and second resonant frequencies from 178 to 194 MHz and 370 to 390 MHz, respectively.

Fig. 7 shows the RG_{peak} of the 4-element ODA array with the initial and optimized geometries at boresight. The results show that the RG_{peak} of the optimized design is insignificantly reduced, i.e., 0.3 dBi lower-than that of the initial design.

A parametric study was performed on the optimized design to observe the effect of the S_{wing} and S_{para} on the antenna performance. Fig. 8 shows the simulated active VSWR of the elements 1 and 2 for changing S_{wing} from 250 to 290 mm and S_{para} from 44 to 52 mm. As the S_{wing} increases, the VSWR of the element 1 is reduced across the whole band, but the last crossing frequency of the active VSWR below 2 (f_{last}) of element 2 rapidly degrades from 500 to 440 MHz, despite slightly lower VSWR in the frequency range from 250 to 400 MHz. Similarly, with an increase of S_{para} from 44 to 52 mm, the VSWR of the element 1 decreases in the desired frequency range, while the f_{last} of the element 2 is reduced from 488 to 458 MHz. Unlike the similar trend of VSWR for S_{wing} and S_{para}, the
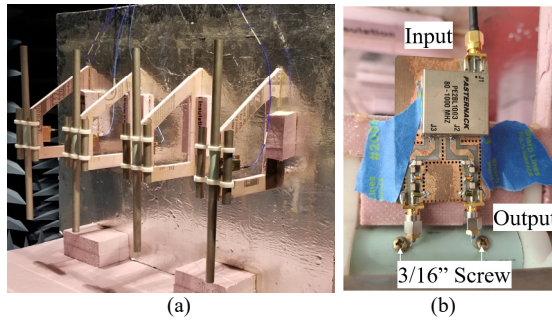
Fig. 10. (a) Fabricated 4-element open-sleeve dipole antenna array under the FOAMULAR sheet and (b) connection between antenna and balun.
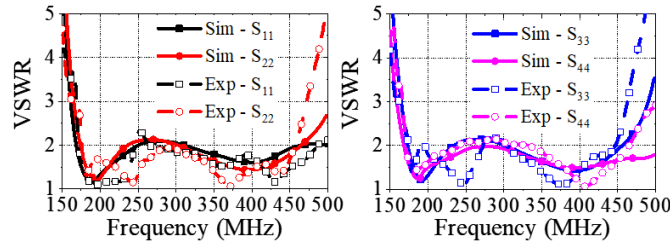

Fig. 11. Simulated and measured active VSWR of the 4-element open-sleeve antenna array.

trends of the RG_{peak} for various S_{wing} and S_{para} were different, as illustrated in Fig. 9. As the S_{wing} increases, the RG_{peak} above 400 MHz decreases significantly, while there is no change for various S_{para}. Table I summarizes the optimized specifications and dimensions.

III. EXPERIMENTAL RESULTS

The 4-element ODA array was fabricated based on the dimensions and specifications in Table I and characterized for antenna performance to compare to the simulation results. Fig. 10 shows the fabricated 4-element ODA array on top of the FOAMULAR foam with an aluminum (Al) sheet and connection between antenna and balun. The dipole is excited by a 3/16" metal screw on each dipole, separated by 30 mm as shown in Fig. 1, and a short wire between the antenna and balun. To hold the separated dipole elements, G10-FR4 fiberglass epoxy laminate (relative permittivity of 4.8 and dielectric loss tangent of 0.0017) was used [9]. A high-density polyethylene connector piece was used to hold the dipole and parasitic element in one piece. For the aircraft wing, a 1000 mm long x 2750 mm wide x 5 mm thick FOAMULAR foam with the Al sheet was utilized. All antenna performances were characterized in an anechoic chamber.

Fig. 11 shows the simulated and measured active VSWR of the optimized 4-element ODA array. The simulation result, especially when the VSWR crosses 2, agreed reasonably well with the measured results. As Fig. 11 clearly shows, the measured VSWR is below 2.1 in the desired frequency range of 170 to 470 MHz. The small discrepancy between the measured and simulated results is attributed to the insertion of a wire between the balun and dipole and fabrication imperfections.

Fig. 12 illustrates the simulated and measured normalized realized gain of the 4-element ODA array at 200, 320, 400, and 470 MHz. The fabricated array exhibits similar performances compared to the simulated array. A slight discrepancy between
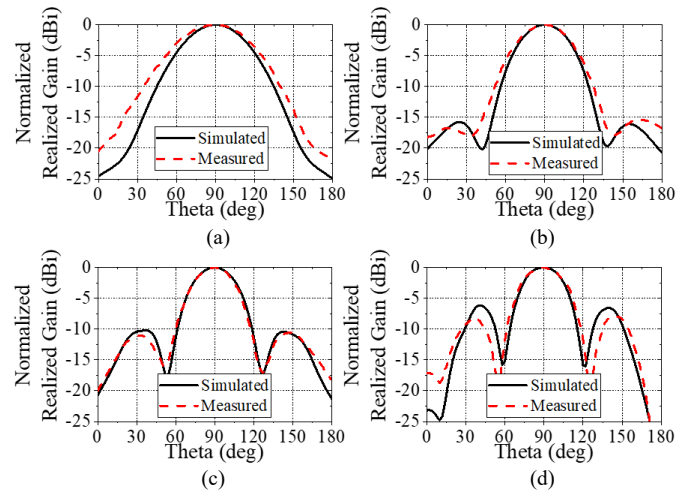

Fig. 12. Simulated and measured realized gain of the 4-element open-sleeve antenna array at (a) 200, (b) 320, (c) 400 and (d) 470 MHz.
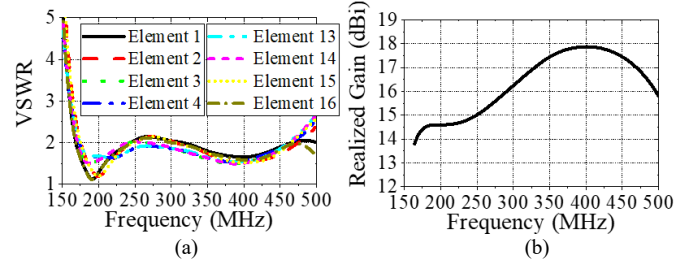

Fig. 13. Simulated (a) active VSWR and (b) realized gain at boresight of the 16-element open-sleeve antenna array.

the measured and simulated results is due to the misalignment between the array and reference antenna.

The required minimum RG_{peak} (RG_{peak_min}) is 10 dBi. However, the simulated RG_{peak_min} of the 4-element ODA array was 7.5 dBi. Thus, to increase RG_{peak_min}, the ODA array with higher N_{ant} is investigated. An aerodynamic and aircraft study shows that each wing could sustain 16 ODAs. The dimensions of elements 1 and 4 are used for the edge elements' dimensions, i.e., elements 1 and N_{ant}. For the other elements, the dimensions of elements 2 and 3 are used. Fig. 13 shows the simulated active VSWR of element 1-4 and 13-16 and RG_{peak} of the 16-element ODA array. In Fig. 13, only VSWR of element 1-4 and 13-16 are shown to provide more clear plots. The results show that all elements exhibit a VSWR below 2.1 and a RG_{peak} of 14-18 dBi.

IV. CONCLUSION

An ultrawideband and simple VHF/UHF 4-element open-sleeve dipole antenna array was developed, optimized, fabricated, and characterized for airborne ice measuring radar. The optimized 4-element array exhibits a VSWR below 2.1 in the desired frequency range of 170 to 470 MHz with a peak realized gain up to 12 dBi. A higher peak realized gain of 18 dBi is achievable when 16 elements are employed with the calculated dimensions.

REFERENCES

[1] P. Glick, J. Clough, and B. Nunley, "Sea-level Rise and Coastal Habitats in the Pacific Northwest," National Wildlife Federation, Seattle, WA, USA, Jul. 2007.

[2] F. Rodriguez-Morales, et al., "Advanced Multifrequency Radar Instrumentation for Polar Research," *IEEE Trans. Geosci. Remote Sens.*, 52 (5), pp. 2824-2842, May. 2014.

[3] A. Fenn, P. Hurst, J. D. Krieger, J. Sandora, and L. Parad, "Ultrawideband VHF/UHF Dipole Array Antenna," in *Proc. Int. Symp. Phased Array Syst. Technol.*, Waltham, MA, USA, 2010, pp. 79-82.

[4] J. Yan, et al., "A Polarization Reconfigurable Low-Profile Ultrawideband VHF/UHF Airborne Array for Fine-Resolution Sounding of Polar Ice Sheets," *IEEE Trans. Antennas Propag.*, 63 (10), pp. 4334-4341, Oct. 2015.

[5] I. Tzanidis, K. Sertel, and J. Volakis, "UWB Low-Profile Tightly Coupled Dipole Array With Integrated Balun and Edge Terminations," *IEEE. Trans. Antennas Propag.*, 61 (6), pp. 3017-3025, Jun. 2013.

[6] M. Wang, W. Wu, and Z. Shen, "Bandwidth Enhancement of Antenna Arrays Utilizing Mutual Coupling between Antenna Elements," *Int. J. Antenn. Propag.*, pp. 1-9, Jun 2010.

[7] C. A. Balanis, *Antenna Theory-Analysis and Design*, John Wiley & Sons, New York, NY, USA, 3rd edition, 2005.

[8] A. C. Ludwig, "Mutual Coupling, Gain, and Directivity of an Array of Two Identical Antennas," *IEEE Trans. Antennas Propag.*, 24 (6), pp. 837-841, Nov. 1976.

[9] Fasteners, "Plastic materials: FR-4/G10 Plastic Fasteners," Fastenercomponent, Oct. 2015. [Online]. Available: http://www.fastenercomponents.com/news/fr-4-g10/.